Research Updates

Guidelines for superlattice engineering with giant molecules: The pivotal role of mesoatoms

Xiao-Yun Yan,[1,2,*] Yuchu Liu,[1,2,*] Xian-You Liu,[1] Huanyu Lei,[1] Xing-Han Li,[1] Yicong Wang,[1] Weiyi Li,[1] Qing-Yun Guo,[1,2] Mingjun Huang,[2,†] and Stephen Z. D. Cheng[1,2,‡]

[1]*South China Advanced Institute for Soft Matter Science and Technology, School of Emergent Soft Matter, South China University of Technology, Guangzhou 510640, China*

[2]*Department of Polymer Science, School of Polymer Science and Polymer Engineering, University of Akron, Akron, Ohio 44325, USA*

(Received 30 August 2023; revised 4 November 2023; accepted 8 November 2023; published 14 December 2023)

Soft materials with nanostructures, such as Frank-Kasper (FK) and related spherical phases, have garnered significant interest in recent years. However, there is still a lack of rational approaches to design and fabricate these specified spherical phases. This is primarily due to the hierarchical self-assembly that commonly occurs during phase formations, which obscures the correlations between discrete molecules and the resulting superlattices. To address this challenge, giant molecules (GMs), which are macromolecules with precisely controlled chemistry and architecture, present a promising platform to explore the underlying principles of self-assembly. In this contribution, our focus is primarily on the features of the intermediate stage of self-assembly (i.e., mesoatoms) and a review of experimental guidelines in molecular systems to control the characteristics of self-assembled phases. We will first introduce the experimentally accessible spherical phases up to the current stage. The phases are categorized based on their structural features, including the simple spherical packing phases, FK phases, quasicrystalline phases, and quasi-FK phases. Subsequently, we will delve into the mesoatomic parameters that can be experimentally controlled, including the individual size (V), size difference (ν), stoichiometry (ϕ) and size distribution ($Đ_{size}$) of mesoatoms. By envisioning the perspective from mesoatoms of GMs, we aim to facilitate the construction of spherical phases through rational molecular designs.

DOI: 10.1103/PhysRevMaterials.7.120302

I. INTRODUCTION

Metals and their alloys lay the foundation of human civilization. By alloying metals, countless properties emerge from a handful of metallic elements. Particularly, brass and bronze, although the two materials share the common base metal, they display distinct behaviors in strength, ductility, luster, conductivity, and melting temperature. Nowadays, it is understood that materials' properties not only are determined by the constituent elements but also by the spatial arrangement of these elements. For instance, materials with mesoscale periodic structures would display vastly different photonic [1–3] acoustic/phononic [4,5], and mechanical properties [6,7], even though they are with identical compositions. As top-down fabrication techniques have reached their limit at scales below 10 nanometers [8–11], there has been a growing emphasis on bottom-up approaches [12–14]. These approaches involve the spontaneous assembly of nanobuilding blocks into complex superlattices. Consequently, it has become increasingly imperative to understand the packing phenomena of nanobuilding blocks [15].

One bottom-up strategy to prepare alloy mimics is to pack magnified atom analogues, like nanocrystals [21–25], microbeads [24,26,27], and proteins/DNA complexes [28–30] into their superlattices. During this process, self-assembly can be monitored, either using scattering technologies or microscopic techniques, and simulated with relative ease. The ability to capture the entire process makes it convenient to establish correlations between the "input" parameters of the building blocks (e.g., size, shape, and functionality of colloids) and the resulting "output" packing structures. Another class of material is molecule-based systems (block copolymers, dendron/dendrimers, small-molecular surfactants, GMs). In many cases of molecule-based systems, the nonrigidity (i.e., molecular feature that with degrees of freedom for conformational changes on a global scale) allows solvent-free assembly as well as fast lattice-forming kinetics (though exceptions exist in systems as in Refs. [31,32]); these materials also ensure the feasibility in chemical modification and scalable preparation [33–35]. However, different from colloidal particles with a fixed size, self-assembly of molecules into a superlattice is a hierarchical process. Macromolecules first self-assemble into molecular clusters, upon which the superlattice is constructed (Fig. 1). This stepwise organization, combined with the absence of direct observation techniques, makes the "input-output" correlation less straightforward. This challenge arises from the fact

*These authors contributed equally to this work.
†Corresponding author: huangmj25@scut.edu.cn
‡Corresponding author: scheng@uakron.edu

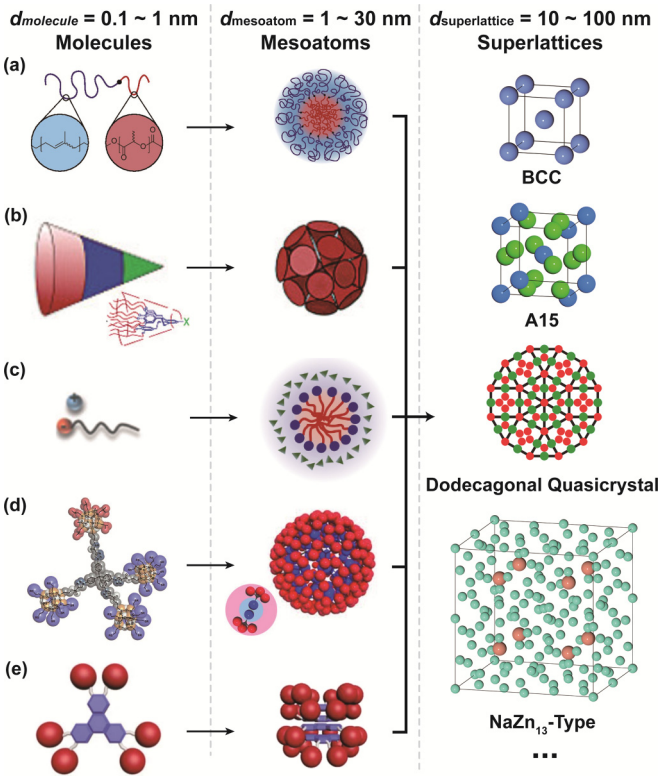

FIG. 1. Hierarchical self-assembly based on various materials systems, intermediated by mesoatoms, results in various spherical packing superlattices. The material systems include (a) block copolymers (Reproduced with permission from Ref. [16]; Copyright (2014) National Academy of Sciences), (b) dendritic molecules (Reproduced with permission from Ref. [17]; Copyright (1997) American Chemical Society), (c) surfactants (Reproduced with permission from Ref. [18]; Copyright (2017) National Academy of Sciences), and giant molecules with (d) polyhedral (Reproduced with permission from Ref. [19]; Copyright (2015), American Association for the Advancement of Science) or (e) polygonal designs [Reproduced with permission from Ref. [20]; Copyright (2019) Springer Nature (London)].

that characteristics of self-assembled superlattices (unit cells' symmetries, dimensions, etc.) can decouple from the parameters at molecular level (molecular sizes, shapes, etc.) during the intermediate stages. As the intermediate clusters form, conformations of individual molecules become averaged, molecular symmetries are rearranged, and molecular polarities are neutralized. The intermediate molecular cluster is known as mesoatoms due to their analogous role to atoms in atomic crystals [36,37]. This concept is borrowed from colloidal particle systems and has gained wider acceptance in the field of self-assembly. More recently, this concept was extended to describe the grouping of molecules that serve as repeating units in networklike structures, greatly facilitating the description of these complex structures [38].

In soft materials, people never stopped searhing for correlation between the molecular structures and obtained phases. One good example is the block copolymer system. By manipulating molecular weight, incompatibility among blocks, volume asymmetry, and conformational asymmetry, people

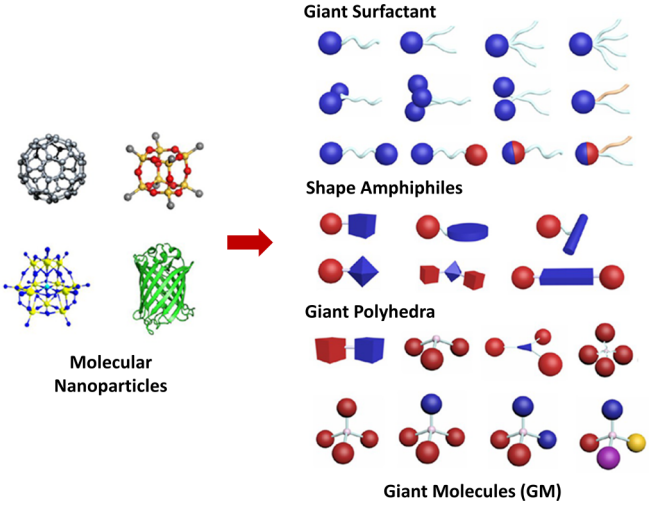

FIG. 2. Key components and general structures of giant molecules (GMs). (Reproduced with permission from Ref. [45]; Copyright (2014) American Chemical Society).

could control the microphase separation of two blocks, leading to lamellar, bicontinuous, columnar, or some spherical phases [39]. These factors have been extensively reviewed in previous contributions [13,40–44]. However, when the disconnections caused by hierarchical self-assembly process stands out, as in spherical packings, the correlations become vaguer than other phases. As such, giant molecules (GMs, Fig. 2) [45–49], a class of macromolecules featuring in precise molecular architecture, have garnered much attention. Unlike block copolymers, GMs are constructed using nanosized, well-defined fragments (e.g., polygonal molecular cores, or polyhedral nanocages with different functionalities) that do not necessarily need to be chainlike submolecular units (e.g, polymers, oligomers, or alkyl chains). By adopting GMs, researchers could access a exceptionally broad and precisely controlled parameter space of molecular architecture, enabling the versatile exploration of phase behaviors in the bulk state [8,19,20,33,34,48,50–72].

In this contribution, we put our major focus on characteristics of mesoatoms and how these characteristics bridge the information from molecules to superlattices. In deliberating these issues, we utilize GMs as examples for their structural precision is at molecular level. Although many theoretical guidelines have been proposed [39,73–76], we would primarily review the guidelines that have been tested in experimental studies of bulk materials. To this end, we first introduce the experimentally accessible phases up to the current stage. The phases are categorized based on their structural features, including the simple spherical packing phases, Frank-Kasper (FK) phases, quasicrystalline phases, and quasi-FK phases. We then introduce the mesoatomic characteristics that could be experimentally manipulated, including the individual size (V), size difference (ν), stoichiometry (ϕ) and size distribution ($Đ_{size}$) of mesoatoms. Finally, we envision these approaches could transit to molecular systems; we also suggest some opportunities longing to be taken in this field.

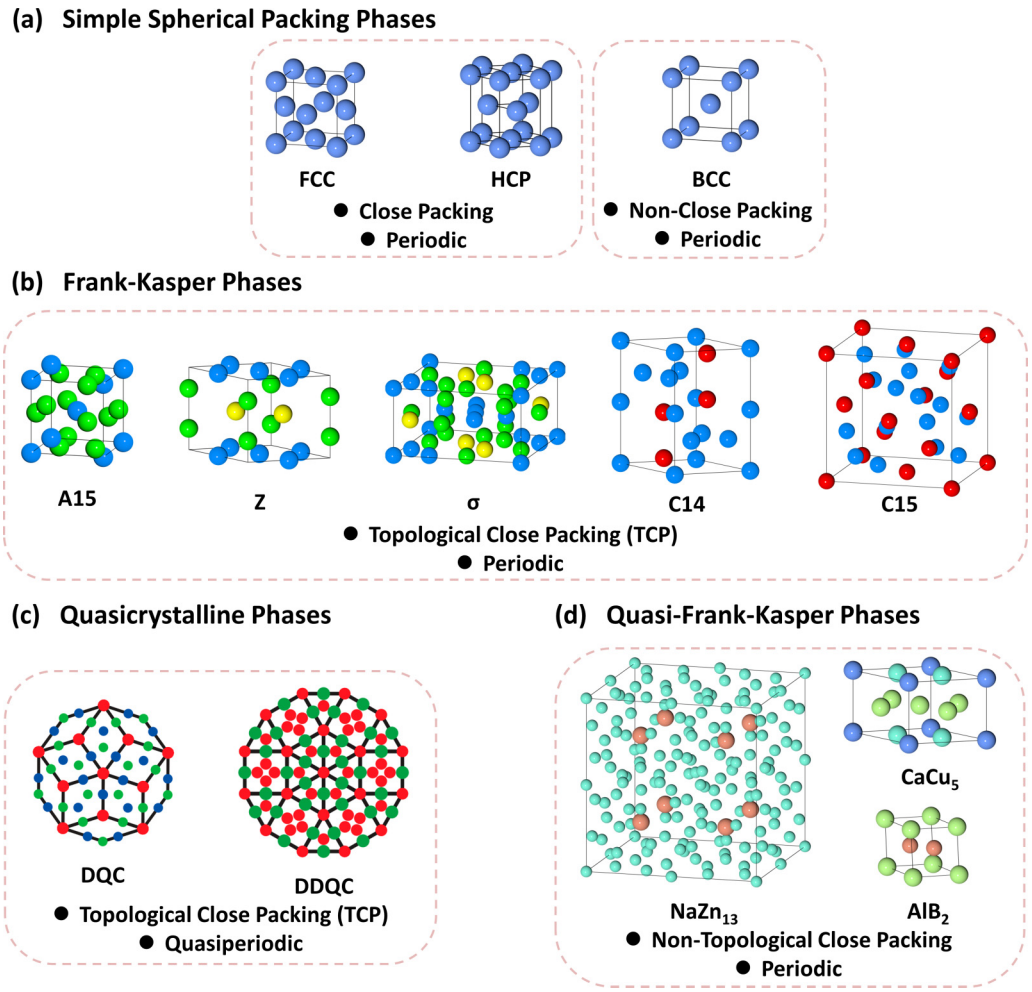

FIG. 3. Illustration of four categories of experimentally accessible phases. Structures and key features of (a) simple spherical packing phases, (b) Frank-Kasper phases, (c) quasicrystalline phases (Reproduced with permission from Ref. [53]; Copyright (2022) National Academy of Sciences), and (d) quasi-Frank-Kasper phases [77]. Each sphere represents a mesoatom in molecule-based superlattices.

II. EXPERIMENTALLY ACCESSIBLE ALLOY-TYPE SUPERLATTICES

To start, our exploration focuses on experimentally accessible spherical phases in molecular systems. We have classified these phases into four main categories: simple spherical packing phases, FK phases, quasicrystal phases, and quasi-FK phases, each exhibiting distinct packing features (Fig. 3). The simple spherical packing phases include face-centered-cubic (FCC) [78–84], hexagonal close-packing (HCP) [82–89], and body-centered-cubic (BCC) phases [8,18,90,91]. These phases possess simple unit cells and commonly occur in the packing of equal-volume spheres. The FK phases discovered in soft matters include A15 [17–20,32,50,52,54,59,61–63,65–70,91–113], Z [20,70], σ [18,32,53,59,61,63,67,71,90,114–117], C14 [31,50,52,54,69,88,118–122], and C15 [31,50,69,88,89,119,120,122–124]. The unit cells of FK phases are more complex, often requiring minor volume fluctuation among spheroidal building blocks. Notably, the compositional spheroids in FK phases always fall in the topologically close packing (TCP) arrangements, characterized by coordination number (CN) of the central sphere equals to 12, 14, 15, or 16. The quasicrystal phases discovered in soft matter are either decagonal quasicrystal (DQC) [53] or dodecagonal quasicrystal (DDQC) [53,59,63,66,67,71,125–132]. These two types of two-dimensional (2D) quasicrystals locally adopt TCP but lack globally 3D translational periodicity [53,133]. Lastly, the quasi-FK phases comprise structures like AlB_2 [50,52,122], $CaCu_5$ [54], $NaZn_{13}$ [50,52,54,56,134], and others. Their local packing arrangements deviate from TCP to accommodate the large volume difference of spheroids while still preserve the translational periodicity. In the following sections, we will provide brief overviews of the key features displayed by these four types of phases.

A. Simple spherical packing phases

Simple spherical packing phases include the BCC, FCC, and HCP phases. These phases are parent structures for a wide variety of metal alloys [135]. They have relatively simple unit cells, and only one type of Wyckoff position is required to describe the unit cell. Both the FCC and HCP phases have a CN of 12. The FCC unit cell differs from HCP by its coordination arrangements: atoms in FCC are coordinated within a

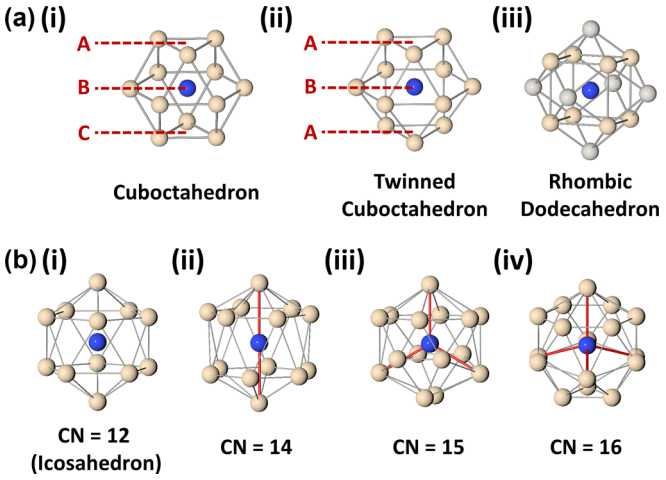

FIG. 4. Coordination environments simple spherical packing phases and FK phases. Coordination environments of (a) (i) FCC, (ii) HCP, and (iii) BCC. (b) The four local coordination environments in TCP, including CN equals to (i) 12, (ii) 14, (iii) 15, and (iv) 16. The central atoms are represented in blue, and peripheral atoms are shown in light yellow. In a(iii), atoms with farther distances to the central atoms are highlighted in gray. In b(ii)–b(iv), skeletal lines connecting nonpentagonal faces are illustrated as red lines.

cuboctahedron [Fig. 4(a)(i)] featuring with a periodic three-layered (ABC) spherical stacking, whereas atoms in a HCP unit cell are within a twinned cuboctahedron [Fig. 4(a)(ii)] with a two-layered (AB) spherical stacking. On the other hand, the BCC phase adopts a CN of 14, with all atoms within a rhombic dodecahedron coordination environment [Fig. 4(a)(iii)]. In a 3D space, the kissing number (i.e., the greatest number of nonoverlapping unit spheres that can be arranged in that space such that they each touch a common unit sphere) is 12 [136]. The local environments of FCC and HCP reach the densest arrangement regarding how many neighboring spheres directly contact the common one. Consequently, the two phases are considered as "close packing" phases. On the contrary, despite BCC (CN = 14) having higher CN than FCC and HCP (CN = 12), 6 of the coordinating atoms [gray spheres in Fig. 4(a)(iii)] are more distant (∼15%) than the 8 others. Therefore, BCC is not considered close packed.

In hard sphere packing, the structure with minimized voids (i.e., highest packing efficiency) is favored. The packing efficiency Φ is defined as V_a/V, where V_a and V represent the volume of the portion occupied by spheres and the entire unit cell, respectively. The highest packing efficiency of equal-volume spheres occurs in FCC or HCP phases ($\Phi \sim 74\%$) [137]. On the contrary, Φ in BCC phases reaches only 68%. Therefore, FCC and HCP phases are prevalent in packing of hard spheres. On the other hand, in the packing of soft spheres, voids would always be filled by deformation of soft mesoatoms, favoring a nonspherical geometry with minimized interfacial area. To assess the degree of a particle's deviation from a perfect spherical shape (i.e., sphericity), researchers typically employ a parameter known as isoperimetric quotient, $IQ = 36\pi V^2/S^3$, where V and S represent volume and surface area of the particle [16,23]. IQ equals 1 when a particle is a perfect sphere. In 1887, Lord Kelvin raised a famous question (i.e., Kelvin's problem): what regular partition of space into cells of equal volume has the smallest surface area of cells? For a long time, people falsely believed the optimal solution for Kelvin's problem was BCC since the IQ of BCC reaches 0.757, higher than most other phases including FCC phase ($IQ = 0.741$) [23]. The BCC's higher IQ value partially accounts for the fact that: in soft materials, though FCC and HCP phases were predicted [74,75,138,139] and discovered [78–89], the dominant packing phase is BCC. However, in the 1990s, people started to realize there are counter-examples of structures to Kelvin's problem with higher IQ values than BCC [140].

B. Frank-Kasper (FK) phases

In FCC and HCP phases (Sec. II A), we explored two forms of spherical packing with the highest kissing number (CN = 12) in 3D space. However, there is another CN = 12 configuration with an icosahedral geometry: 12 atoms surround the common sphere with identical distances and exclusively tetrahedral interstices [Fig. 4(b)(i)] [135]. This packing scheme was considered to be the most stable one in terms of free energy. As such, the special icosahedral coordination was named TCP.

Unfortunately, the icosahedral coordination by itself does not tile a gapless 3D space (as regular pentagons do not tile a 2D plane), which means a crystal cannot solely be based on icosahedral coordination (distinct from the cases in FCC and HCP). Frank and Kasper later demonstrated that icosahedra can be accommodated with three other allowed TCP types of coordination that possess larger coordination numbers in crystals [141,142]. These three types include CN = 14, 15, and 16 [Figs. 4(b)(ii)–4(b)(iv)], all of which are also solely based on tetrahedral interstices. By incorporating these additional polyhedra, icosahedra could be compensated and efficiently fill the entire space. Subsequently, crystal structures consisting of icosahedral coordination and packing arrangements with CN = 14, 15, or 16 were named FK phases.

To the best of our knowledge, 28 types of FK phases were discovered in metal alloys [143,144]. In molecular self-assembled structures, five types (A15 [17–20,50,52,54,59,61–63,65–70,91–113], Z [20,70], σ [18,53,59,61,63,67,71,90,114–117], C14 [31,50,52,54,69,88,118–121], and C15 [31,50,69,88,89,119,120,123,124,145]), of FK phases were experimentally identified [Fig. 3(b)]. Based on building blocks larger than molecules, the structures of FK phases were also probed with nanocrystals [23], colloids [146], and even soap bubbles [147]. The prevalence of FK phases in soft matters infer their thermodynamic stability at different length scales. This is supported by the fact that the optimal solution for Kelvin's problem turned out to be the Weaire-Phelan structure [140] (the dual structure of the A15 phase, $IQ = 0.764$) rather than BCC.

C. Quasicrystal phases

Quasicrystals (QCs) are unique structures characterized by long-range orientational orders and absence of 3D translational symmetry [148]. This feature is also called quasiperiodicity. These quasiperiodic structures can exist in

1D (e.g., Fibonacci lattice), 2D (e.g., Penrose tiling), or 3D (e.g., rapidly solidified Al-Mn alloy) forms [149]. In soft matters, all discovered quasicrystals are 2D quasiperiodic structures [Fig. 3(c)], including the decagonal (tenfold rotational symmetry) QC (DQC) [53], and dodecagonal (12-fold rotational symmetry) QC (DDQC) [53,59,63,66,67,71,125–132] as characterized by the symmetry of the diffraction pattern (or other equivalent expressions in a reciprocal space). Structure-wise, QCs in soft matters are locally TCP (though this may not be true for metallic QCs, like some 3D QCs based on Mackay clusters [150], or Tsai clusters [151]) yet lacking the in-plane periodicity. This packing feature was experimentally confirmed by high-resolution microscopic characterization in DDQC self-assembled by nanocrystals [133]. Therefore, the QCs in soft matter are structurally related with FK phases and are considered as the approximants of some FK phases (e.g., σ phase) [152].

D. Quasi-FK phases

Intermetallic-type phases (usually named after their prototypes, e.g., AlB_2 [50,52], $NaZn_{13}$ [50,52,54,56,134], and $CaCu_5$ [54] phases) emerge in soft material alongside simple packing, FK, and QC phases [Fig. 3(d)]. These phases are classified as quasi-FK phases as proposed by Travesset [77].

Structurally speaking, quasi-FK phases are characterized as non-TCP, meaning they have CNs other than 12, 14, 15, or 16, yet they retain global periodicity. Their local structures, however, are closely related to TCP. As described in Sec. II B, the introduction of coordination environments with CN = 14, 15, or 16 facilitates gapless packing of icosahedral units. These augmented CNs result from coordination forms with CN = 12 that are defected by a specific type of disclination [disclination angle $-2\pi/5$, with the directions of disclinations outlined as red lines in Figs. 4(d)(ii)–4(d)(iv)]. Consequently, the structures of FK phases can be treated as a specific combination of disclination lines [153]. By introducing disclinations with mathematically equivalent expressions to FK phases, quasi-FK phases are formed. The presence of non-TCP local packing becomes inevitable when the size difference of coexisting mesoatoms in a unit cell becomes increasingly large. In such cases, achieving TCP-type CNs (12, 14, 15, or 16) becomes impractical, as they are too low for large motifs to contact with as many as small ones, yet too high for small motifs if they are contacted with large ones. Quasi-FK phases prevalently exist in nanocrystal systems and started to be recognized in molecular systems as well [50,52,54,134]. To date, all quasi-FK phases discovered in molecule-based systems (AlB_2, $NaZn_{13}$, and $CaCu_5$ phases) are with minimal difference in disclinations from TCP (as characterized by degree of icosahedral order proposed in Ref. [77]).

III. GUIDELINES IN FABRICATING SUPERLATTICES FROM THE PERSPECTIVE OF MESOATOMS

In molecule-based spherical packing phases, self-assembly occurs primarily in a hierarchical manner, wherein multiple molecules come together to form micellar intermediates, also known as mesoatoms, which serve as the building blocks for the resulting superlattices. During the formation of mesoatoms, the individual molecules' anisotropy in chemical structures is largely diminished. Additionally, experimental treatments, such as thermal annealing, directly induce the self-assembly of disordered molecules into a periodic superlattice, making the mesoatoms inseparable throughout the entire process. These factors contribute the challenges in predicting the characteristics of the resulting superlattices. The pivotal roles of mesoatoms spur us to ask: (1). How do the features of individual molecules influence the characteristics (i.e., individual size (V), size difference (ν), stoichiometry (ϕ), and size distribution ($Đ_{size}$) of mesoatoms) of mesoatoms? (2). How do the properties of mesoatoms dictate the structures of superlattices? The principles of design that we have described in this context revolve around addressing these two fundamental aspects. Our hope is that by considering the perspective of mesoatoms, researchers can better understand and rationally fabricate desirable spherical packing systems.

A. Volume of mesoatoms (V)

The size of a mesoatom is determined by the geometry of its compositional molecules. To create a mesoatom, the volume of two incompatible blocks within one molecule must be significantly different, resulting in a conelike molecular geometry [Fig. 5(a)] [61,64,66]. For ease of discussion, we categorize the segments in a conelike molecule into three basic types: tip, linker, and tail [Fig. 5(a)]. In a spherical mesoatom, conelike molecules arrange themselves tip-to-tip [Fig. 5(c)]. Additionally, besides conelike geometry, researchers also consider molecules with disklike geometry [Fig. 5(b)] [50,71]. However, it is essential to note that disklike geometry is intrinsically composed of circularly arranged conelike segments [one outlined by the red dash in Fig. 5(d)]. Therefore, to understand how mesoatomic sizes are determined, one should focus solely on evaluating the features of conelike molecules/segments.

Two molecular parameters are involved in describing the features of a conelike unit. Firstly, the tip-to-tail distance [l, Fig. 5(a)] can be experimentally altered by changing the length of the branch (e.g., by shortening or elongating the linker). Second, the variable cone angle [θ, Fig. 5(a)] can be controlled by manipulating the branching of molecules (e.g., by tethering fewer or more tails to the tip). Modifications to θ or l led to changes in mesoatomic features, similar to the effects observed in dendritic systems [154,155].

When l increases, the size of the resulting mesoatom becomes larger, which also yields a larger unit cell. For example, Z. Su *et al.* prepared a series of disklike molecules [Tp-Ph-C_n-6BP, models illustrated in Fig. 5(e)(i)] with different linker lengths ("n", the number of methylene (-CH2-) groups in the linker part varies from 3 to 10), while their cores (Tp, triphenylene) and tails remained identical (BP, BPOSS) [71]. By elongating the linker length, though all molecules self-assembled into BCC phase, the lattices displayed increasing lattice dimension. For Tp-Ph-C_3-6BP whose linker is the shortest, the dimension of cubic lattice (a) is 5.08 nm [small angle x-ray scattering (SAXS) data in Fig. 5(e)(ii)], yet for Tp-Ph-C_{10}-6BP, a equals 6.56 nm [SAXS data in Fig. 5(e)(ii)]. One could also estimate the molecular number

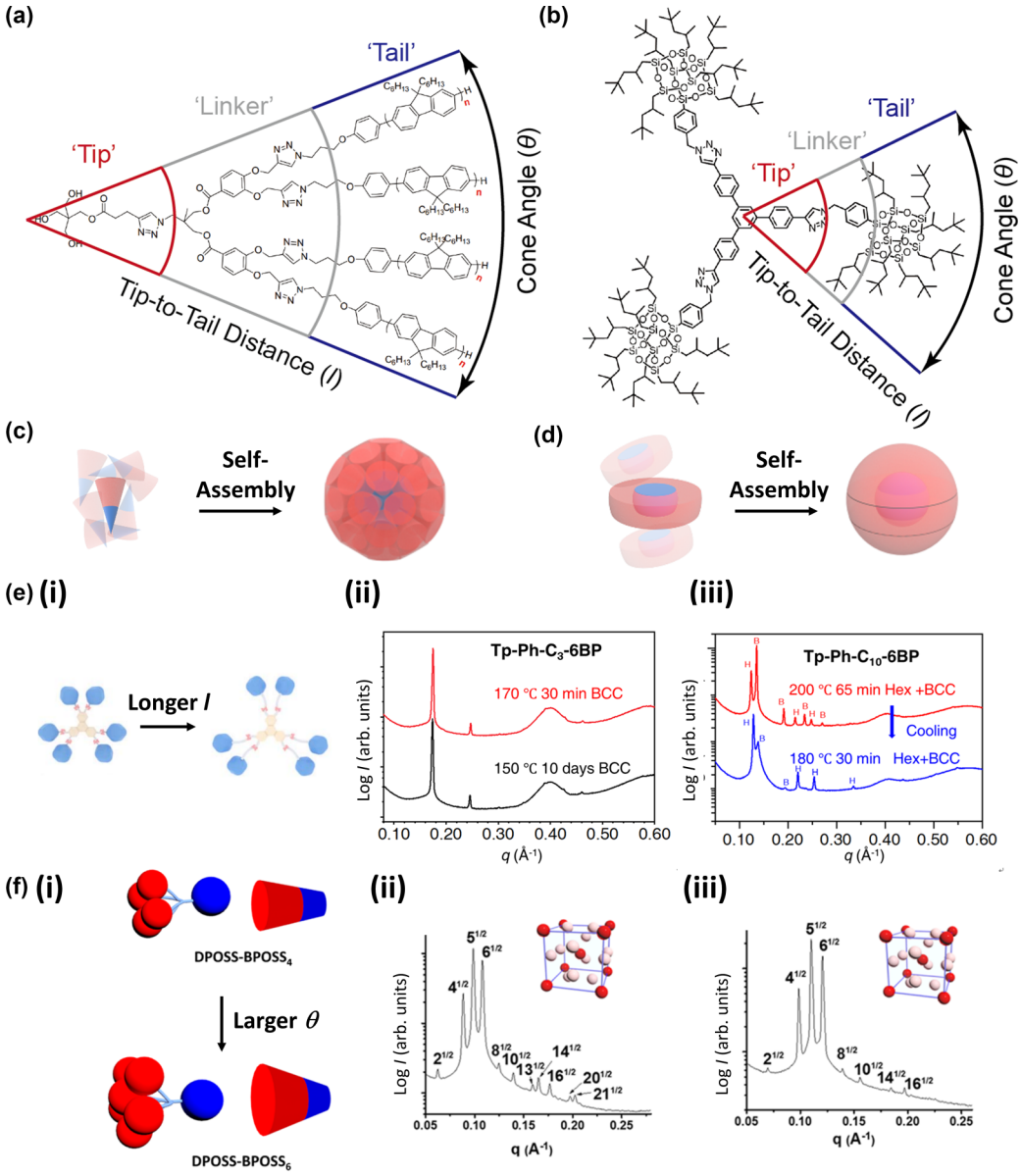

FIG. 5. Effects originated from volume of mesoatoms (V). Chemical structure of a representative (a) conelike (Reproduced with permission from Ref. [66]. Copyright (2019) Wiley-VCH GmbH) and (b) disklike GM. The structure is generally divided into tip, linker, and tail parts based on their locations in the molecular cone in (a). The cone angle (θ) as well as the tip-to-tail distance (l) is also labeled accordingly. (c) Schematic illustration of mesoatoms formed by conelike molecules. (d) Schematic illustration of mesoatoms formed by disklike molecules. (Reproduced with permission from Ref. [50]. Copyright (2021) American Chemical Society). (e) Enlarged unit cell resulted from elongated l. (i) 3D Models of molecular structures before and after elongating linker. (ii) SAXS pattern of Tp-Ph-C_3-6BP whose linker is shorter. (iii) SAXS pattern of Tp-Ph-C_{10}-6BP whose linker is longer. (This figure has been published in CCS Chemistry 2020; "Constituent Isomerism-Induced Quasicrystal and Frank-Kasper σ Superlattices Based on Nanosized Shape Amphiphiles" is available online at 10.31635/ccschem.020.202000338) (f) Smaller unit cell resulted from larger θ. (i) 3D Models of molecular structures before and after enlarging the branchness of tails. (ii) SAXS pattern of DPOSS-$BPOSS_4$ with four BPOSS tails. (iii) SAXS pattern of DPOSS-$BPOSS_6$ with 6 BPOSS tails. (Reproduced with permission from Ref. [64]. Copyright (2019) American Chemical Society).

in one mesoatom (μ) through the lattice dimension. For a cubic unit cell, the μ value is characterized by $\frac{\rho a^3 N_A}{nM}$, where ρ is density of material, n is number of mesoatoms in one unit cell, M is molecular weight of the individual molecule, and N_A is Avogadro's number. After increasing the linker length, the μ increased from ~7 to ~14. Considering the unit cell volume of longer molecules (Tp-Ph-C_{10}-6BP) is 215% of that for shorter molecules (Tp-Ph-C_3-6BP), and linkers take <10% volume of the molecules, the major contribution to the overall volume expansion should be the augmented μ.

On the other hand, increasing the θ may result in a decrease in the dimension of unit cells, as observed in the AB_n dendronlike GMs. Feng *et al.* conducted a study using a series of molecules denoted as DPOSS-$BPOSS_n$, where one hydrophilic head (DPOSS) was tethered to n hydrophobic

tails (BPOSS) [Fig. 5(f)(i)] [61]. For the series $n = 4 - 6$, all samples self-assembled into A15 phase. However, the molecule with less BPOSS ($n = 4$) has a larger lattice dimension [$a = 14.27$ nm, SAXS data in Fig. 5(f)(ii)] than the molecule with more BPOSS [$n = 6$, $a = 12.78$ nm, SAXS data in Fig. 5(f)(iii)]. Interestingly, as n increases from 4 to 6, the volume of the individual molecule increased by 34%, while the unit-cell volume of the superlattice shrank by 28%. This phenomenon could also be rationalized by the change of μ. When n increased from 4 to 6, the μ drop from 44 to 24, representing a 45% loss.

B. Volume difference of mesoatoms (ν)

Ideally, mesoatoms should adopt an optimal molecular number (μ_{opt}) that leads to the lowest free energy. This μ_{opt} value indicates that adding or losing one molecule from a mesoatom may result in either over-crowded packing (greater chain stretch occurring within the nonrigid parts of GMs) or too loose packing (more void space), both of which would thermodynamically destabilize the mesoatom. In a system with uniform μ_{opt}-molecule mesoatoms, there would be no volume difference. However, in a nonideal case, adding one molecule may lead to a slightly loosely packed mesoatom to become slightly over-crowded. The free energy of the two states (μ and $\mu + 1$) would be comparable, resulting in the coexistence of two-sized (larger and smaller) mesoatoms. The two-sized mesoatomic system is characterized by its averaged molecular number per mesoatom ($\bar{\mu} = \frac{n\mu+n'(\mu+1)}{n+n'}$, where n and n' are the number of mesoatoms with μ and $\mu + 1$ molecules, respectively); the size difference of the two-sized mesoatomic system is characterized by volume asymmetry ($\nu = V_l/V_s$, or similarly, by radius ratio of equivalent sphere of mesoatoms, $\gamma = \sqrt[3]{V_s/V_l} = \sqrt[3]{1/\nu}$). The ν equals to 1.0 when mesoatoms are identical in size. Notably, different self-assembly systems exhibit a distinct characteristic range of μ values. Mesoatoms assembled by block copolymers or small-molecule surfactants usually consist of tens or hundreds of molecules, while dendrons/dendrimers typically have μ values greater than 10. In these cases, their ν values are usually very close to 1.0. On the other hand, in many cases of GMs, μ values can be less than 5, which facilitates a wide range of fine-tuning for the ν values.

The volume asymmetry is critically important in determining structural preference. When ν is close to 1.0 (usually < 1.1), the system is more likely to form A15 or σ phase. Once deviating from the low ν region, other FK phases may emerge (e.g., the Z or C15 phase, which are the other two cornerstone FK phases other than A15 [20]). A study conducted by Reddy *et al.* [156] demonstrated that for ν values with neighboring integer ratios ($(\mu + 1)/\mu$), the A15 phase has smaller dimensionless mean areas (a parameter to evaluate how spherical a mesoatom is) when ν = 7:6, 6:5, or 5:4. However, when ν further increases to 4:3 (approximately 1.33), the Z phase emerges [Fig. 6(a)(i)]. To achieve a larger size difference, disklike molecules, whose μ values are usually smaller than conelike molecules, would be a preferred choice (notably, kinetics issues may also endow block copolymers with large ν, but this aspect is beyond the scope of the present review [31]). Experimentally, the Z phase was discovered in self-assembly of Tp-C_0-6BP, a disklike molecule with a triphenylene core and six BPOSS on the periphery [20]. Once annealed at 170 °C, mesoatoms with binary sizes ($\nu = 4 : 3$) spontaneously form and pack into the Z phase [Fig. 6(a)]. The key factor here is that Tp-C_0-6BP has an extremely short linker, largely decreasing the l value (described in Sec. III A) and pushing the mesoatom into a low-μ region. Following a similar approach, Huang *et al.* developed a strategy to increase ν by shrinking the core [70]. In the series n-C_1-6OP (molecules with n-type aromatic core connected to six aliphatic OPOSS cages), by shrinking the size of core part, the average μ drops from 4.5 to 3.4 leading to an A15-to-Z phase transition [Fig. 6(b)].

As predicted by theoretical studies [76,156], further increasing the ν beyond the 4:3 limit would lead to other superlattices (e.g., C14/C15 phases or quasi-FK phases). Though decreasing μ by shortening the l works effectively in unary systems, achieving a ν value beyond 4:3 still remains a grand challenge. On one hand, very few molecular systems can form mesoatoms with average μ lower than 3, limiting the range of achievable ν values. On the other hand, spontaneous symmetry breaking that creating large ν (e.g., 3:2) leads to a substantial jump in free energy. To approach higher ν values, a binary system that contains two types of molecules, forming two types of mesoatoms with different sizes, is thus proposed. Particularly, in such binary molecular systems, self-sorting between the two types of molecules plays a crucial role. The self-sorting refers to the phenomenon where, once two molecules are blended, they tend to form their respective mesoatoms from its single component rather than forming hybrid mesoatoms with homogeneous sizes. While nonself-sorting strategies have been successfully deployed in block copolymers, self-sorting enables us to accurately parameterize complex blending systems and depict the experimental phase diagram based on parameters, including ν (as in Refs. [50,52,54,69]). To design a binary system that favors self-sorting, one must enhance the incompatibility of the two blended-in molecules. In general, there are two strategies to achieve such incompatibility. The first strategy involves ensuring that the two molecules are sufficiently different in size [as illustrated in Fig. 7(a)] [69]. Researchers have observed a threshold of the radius ratio (r_c) beyond which self-sorting succeeds; otherwise, non-self-sorting occurs, characterized by a linear change of mesoatomic radius with the change of stoichiometry (as described in the next section) of the two components. The second strategy involves introducing selective interactions (such as hydrogen bonding or a tendency to crystallize, etc.) that bonds one type of molecules and prevent them from mixing with the other type of molecules [as depicted in Fig. 7(b)] [50]. For instance, one may prepare two types of molecules, one with an aromatic core and the other with a hydrophilic tip. Once being blended, the interaction of mesoatomic "cores" are distinct, ensuring the separation of different types of GMs, while the chemical structure of mesoatomic shell remains identical to facilitate the formation of mixed mesoatom assemblies.

These two self-sorting strategies has worked effectively in giant molecules. As first demonstrated by Liu *et al.*, larger and smaller disklike molecules can coassemble into

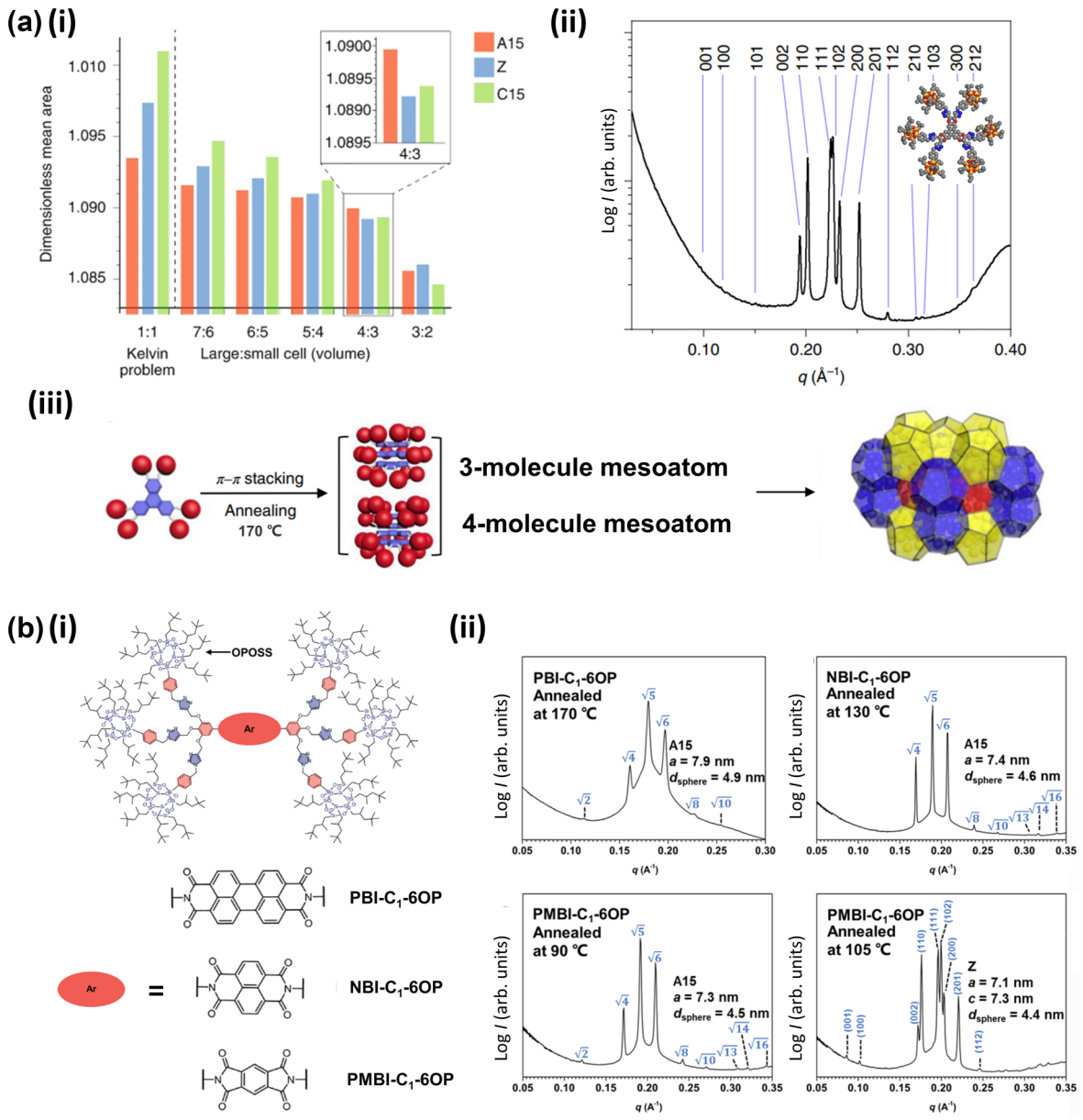

FIG. 6. Effects originated from volume difference of mesoatoms (ν) in unary systems. (a) Z phase formed by GM with high ν. (i) Theoretical structural preference in systems with different volume difference of mesoatoms [Reproduced with permission from Ref. [156]; Copyright (2019) Springer Nature (London)]. (ii) SAXS pattern of the Z phase. (Reproduced with permission from Ref. [20]; Copyright (2019) Springer Nature (London)) (iii) Schematic illustration of how Z phase's formation intermediated by two-sized mesoatoms. (b) Evolution from A15 to Z phase by altering aromatic core size of disklike GM. (i) Chemical structures of PBI-C_1-6OP, NBI-C_1-6OP, and PMBI-C_1-6OP. (ii) SAXS patterns of three GMs with different core sizes. (Reproduced with permission from Ref. [70]. Copyright (2021) American Chemical Society).

unconventional C14 or C15 superlattice [Fig. 8(a)] [69]. For example, the mesoatomic radius r for O-OP24 (24 OPOSS units tethered to the core) is calculated to be 3.08 nm, whereas r equals to 2.62 nm for P-OP10 (10 OPOSS units tethered to the core). The O-OP24 and P-OP10 individually form BCC and A15 phases, respectively. Once the two molecules are blended, self-sorting occurs, and the ν value reaches 1.62, resulting in an unconventional C14 phase. Yan *et al.* further demonstrated that by adopting molecules with different geometries and hydrophilicity (disklike ones which tend to form smaller mesoatoms, while conelike ones which tend to form larger mesoatoms), even higher ν value (from 2.6 to 6.0) could be reached [Fig. 8(b)] [50], exhibiting a region of quasi-FK phases (AlB_2 and $NaZn_{13}$ superlattices) in molecular-based materials [Fig. 8(c)]. This study also suggests that the phase behavior in molecular systems can be bridged to the superlattices in nanoparticle systems. Recently, Wang *et al.*, [54] and Lei *et al.* [52] have also demonstrated the capability of binary blend in constructing other novel quasi-FK phases, including the $CaCu_5$ phase.

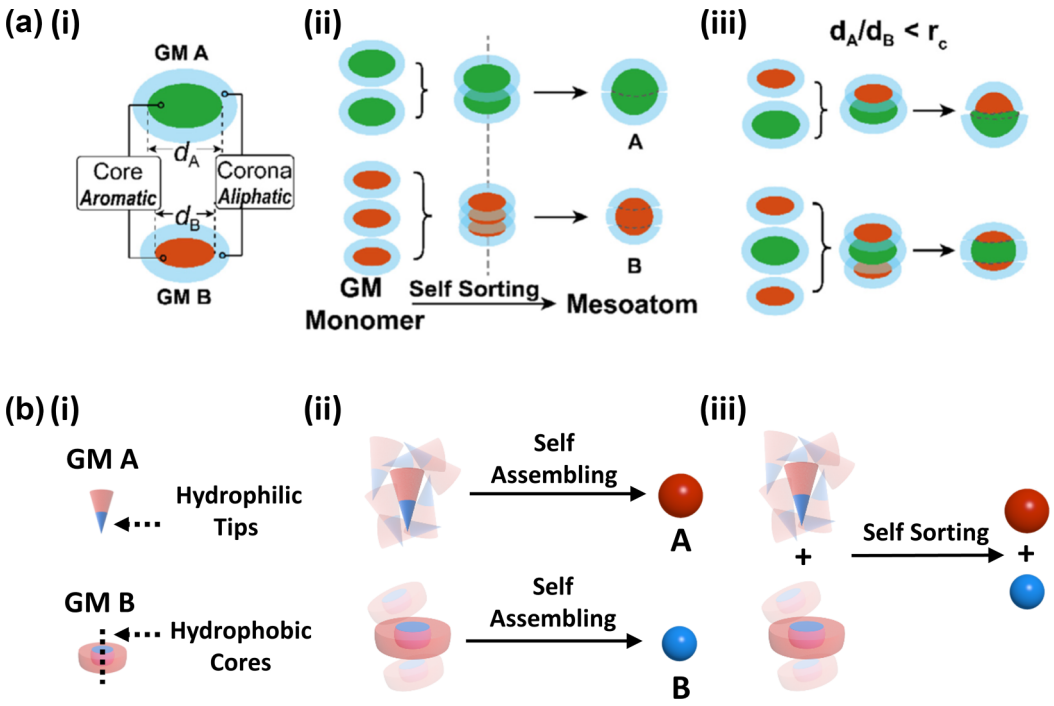

FIG. 7. Two strategies to design a self-sorting binary system. (a) Strategy of mismatch molecular size. (i) Structure and interactions of two types of GMs in different sizes. (ii) Formation of mesoatoms by size driven self-sorting. (iii) Two possible ways of formation of mixed mesoatom when the radius ratio of mesoatoms is beyond the critical value. (Reproduced with permission from Ref. [69]. Copyright (2020) Elsevier Ltd.) (b) Strategy of distinct interactions. (i) Structure and interactions of two types of GMs with different hydrophilicity at tip/core part. (ii) Formation of mesoatoms with different sizes in a unary system. (iii) Formation of mesoatoms with different sizes in a binary blend. (Reproduced with permission from Ref. [50]. Copyright (2021) American Chemical Society).

C. Stoichiometry of mesoatoms (ϕ)

To date, all spherical packing phases are with intermetallic prototypes. For example, the A15 phase corresponds to a Cr_3Si prototype, indicating a mole ratio of 3:1 between chromium and silicon. Similarly, the quasi-FK $NaZn_{13}$ phase suggests the mole ratio of 1:13 between sodium and zinc. In the context of A_nB_m-type intermetallics, the stoichiometry ($\phi = n : m$) reflects the relative amounts of two types of atoms (A and B) in the structure. Similarly, in A_nB_m-type molecule-based superlattices, the stoichiometry should mirror the mole ratio among mesoatoms. In single-component systems, the ϕ values of two-sized mesoatoms are originated from a spontaneous volume bifurcation. In contrast, ϕ values in binary blending systems could be controlled by the molarities of blended molecules. It is essential to note that ϕ considered here pertains to the numbers of mesoatoms rather than the molecules themselves. To gain a better understanding of this concept, let us consider an example involving two types of mesoatoms (A and B) formed by two types of molecules (a and b), respectively. Assuming mesoatom A has a molecular number of $\mu = 100$, and mesoatom B is with $\mu = 10$, to achieve a $\phi = 1 : 1$ between mesoatoms A and B, the mole ratio between molecule a and b should be 10:1. If molecules a and b have identical molecular weights, the actual weight of materials that should be blended into the system would differ by 10 times.

Experimentally, ϕ would be equally important with ν in binary systems. To fabricate a desirable spherical phase, one must determine both ϕ and ν [as illustrated in Fig. 7(c)]. Yan *et al.* have demonstrated different structural preference changing with ϕ in three binary systems [50]. Taking the B-OP_4/H-OP_3 binary system as an example, when ϕ equals to 2:1 the system yields an AlB_2 type of structure; however, once the ϕ increase to 13:1, the $NaZn_{13}$ phase emerges [Fig. 9(a)]. This tendency aligns well with the intermetallic prototypes. In another study demonstrated by Wang *et al.*, the ϕ at which $CaCu_5$ phase emerges also generally tally with the stoichiometry of atoms in their prototypes [Fig. 9(b)] [54].

D. Volume distribution ($Đ_{size}$) of mesoatoms

Though ν and ϕ provide straightforward descriptions of mesoatoms' characteristics, they fall short when multiple types of mesoatomic sizes coexist. In such cases, neither ν nor ϕ could accurately depict the mesoatomic ensemble. Therefore, size distribution of mesoatoms ($Đ_{size}$) becomes a crucial consideration. It is important to clarify that when we refer to $Đ_{size}$, we are discussing the size distribution of mesoatoms, rather than molecules. In the context of the researches presented in this paper, the majority of the GMs exhibit monodisperse molecular weights and well-defined chemical structures. As such, in most cases, the size distribution of mesoatoms derived from GMs remains narrow, as evidenced by the formation of low ν phases (e.g., BCC phases). In addition, having some level of polydispersity in molecular weight (as the case of block copolymers) does not necessarily result in mesoatoms with a broad $Đ_{size}$. To achieve

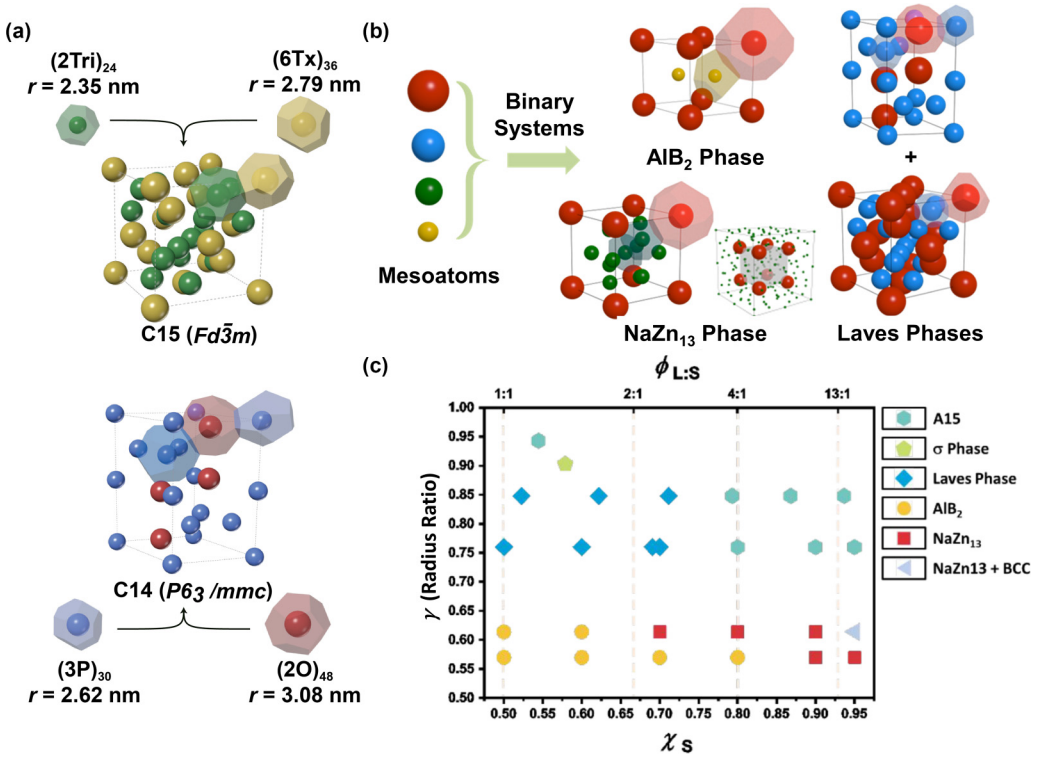

FIG. 8. Effects originated from volume difference of mesoatoms (ν) in binary systems. (a) Laves C14 and C15 phases formed in binary blends of GMs with $\nu \sim 1.6$. Volumes of mesoatoms are labeled accordingly. (Reproduced with permission from Ref. [69]. Copyright (2020) Elsevier Ltd.) (b) AlB_2, $NaZn_{13}$ as well as Laves phases formed in binary blends of GMs with ν in a range from 2.6 to 6.0. Volumes of mesoatoms are labeled accordingly. (c) Phase preference at different radius ratio $\gamma = \sqrt[3]{1/\nu}$. (Reproduced with permission from Ref. [50]. Copyright (2021) American Chemical Society).

a broad $Đ_{\text{size}}$, the molecular structure need to be deliberately designed.

In a giant molecule system, one experimentally viable approach to construct broad $Đ_{\text{size}}$ of mesoatoms is by introducing incomplete self-sorting. As described in Sec. III B, self-sorting of molecules leads to a large ν of mesoatoms. In an ideal case, a blend of molecule A and B spontaneously self-sorts into mesoatoms solely based on pure A and pure B, respectively. As a result, a binodal size distribution is obtained. However, when molecules do not completely self-sort and present partial miscibility, A-B hybrid mesoatoms with intermediate sizes would form yielding a series of mesoatoms with multiple and discrete sizes (Fig. 10). For example, in a binary system presented by Liu *et al.*, two highly alike GMs are

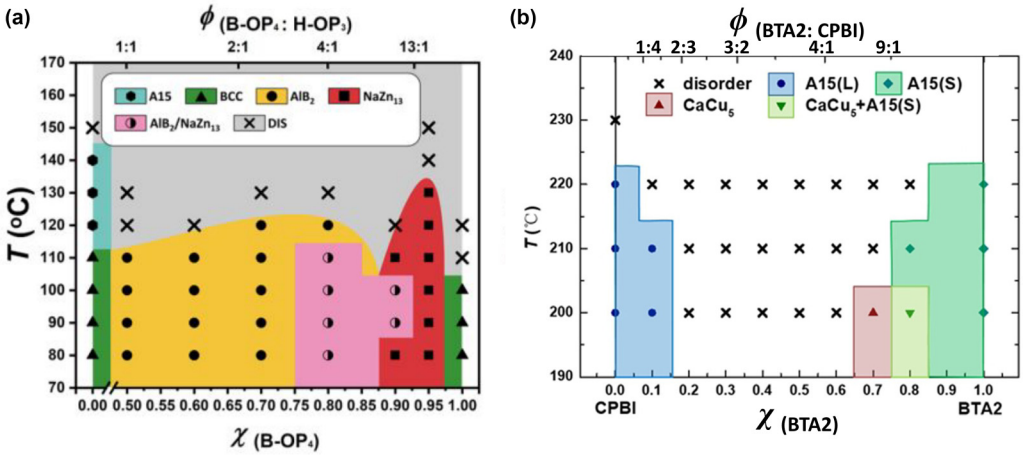

FIG. 9. Effects originated from stoichiometry of mesoatoms (ϕ). (a) Stoichiometry-temperature phase diagram of B-OP_4/H-OP_3 binary system. (Reproduced with permission from Ref. [50]. Copyright (2021) American Chemical Society). (b) Stoichiometry-temperature phase diagram of BTA2/CPBI binary system. (Reproduced with permission from Ref. [54]. Copyright (2022) Wiley-VCH GmbH).

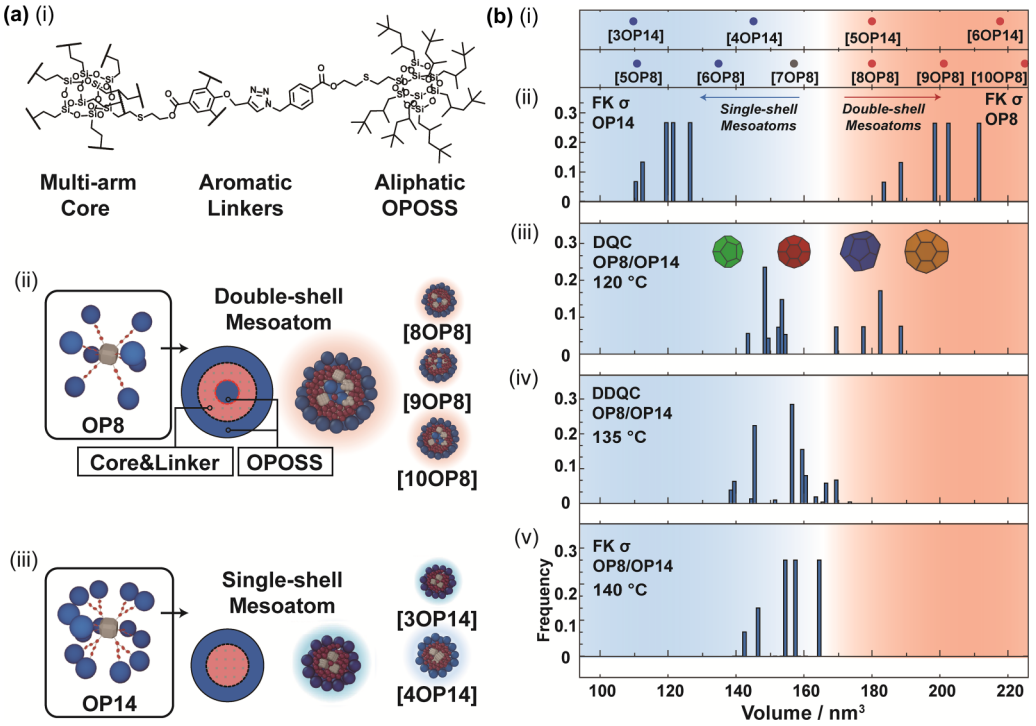

FIG. 10. Size distribution of mesoatoms in an incomplete self-sorting system. (a), (i) Chemical structures and molecular components of OP8 and OP14. (ii) Molecular model of OP8 and its hierarchical self-assembling procedure to FK σ phase. (iii) Molecular model of OP14 and its hierarchical self-assembling procedure to FK σ phase. (b) Calculated volumes and the stable packing models of unblended mesoatoms [xOP8] and [yOP14]. (i) The volume distribution of reconstructed WS cells for FK σ by pure OP14(Left) and pure OP8 (Right). (ii)–(v) The Wigner-Seitz (WS) cells volume distribution of DQC, DDQC, and FK σ assembled by blends of OP8/OP14 at mass ratio = 1:2. (Reproduced with permission from Ref. [53]; Copyright (2022) National Academy of Sciences).

blended [53]. The two molecules have the identical core yet with different numbers of OPOSS tethered around [denoted as OP8 and OP14, respectively, general chemical structure presented in Fig. 10(a)(i)]. In unary systems, both GMs form σ phase, whereas the two phases are composed of mesoatoms with different averaged V [raised from the different molecular packing structure within mesoatoms, i.e., the double-wall model for OP8 and single-wall model for OP14, Figs. 10(a)(ii) and 10(iii)]. Once blended, OP8 and OP14 tend to mix to a certain degree during their aggregation into mesoatoms. Then the hybrid mesoatoms [xOP8/yOP14] with different sizes which depend on the exact value of x and y will be formed. As a result, a DQC→DDQC→σ phase sequence with increasing annealing temperature was observed. By simulating the stable packing models of mesoatoms [xOP8/yOP14] at different compositions [Fig. 10(b)(i)], the authors identified three mesoatomic volume zones, favoring the single-shell, transitional, and double-shell packing modes [as colored by blue, white, and red zones in Figs. 10(b)(ii)–10(b)(v), respectively]. Within this frame, the mesoatomic compositions in the blending assemblies are further studied: the DQC demonstrates an unusually wide volume distribution [Fig. 10(b)(iii)] containing both single-shell and double-shell mesoatoms. The phase later transforms into the DDQC. This is because the majority of double-shell mesoatoms diminishes, affording the DDQC structure with a narrower mesoatomic volume distribution [Fig. 10(b)(iv)]. As the structure evolves into the final stable FK σ phase, the distribution further unifies [Fig. 10(b)(v)].

IV. SUMMARY AND OUTLOOK

Rationally designed alloylike phases demand a comprehensive understanding of the relationship between molecular building blocks and the resulting spherical phases. In this pursuit, we emphasize the pivotal roles of mesoatoms, and highlighted that the precisely controlled parameters of GMs would help to gain more insights into the correlation between molecules and mesoatoms. In this context, we introduced four types of experimentally accessible spherical packing phases: simple spherical packing phases, FK phases, QCs, and quasi-FK phases. Furthermore, we discussed essential mesoatomic parameters that can be experimentally altered, including their individual volume (V), volume difference (ν), stoichiometry (ϕ) and size distribution ($Đ_{\text{size}}$). By comprehending these manipulable parameters in mesoatoms, we can more effectively design molecular structures to achieve desirable superlattices.

However, there are still open questions that need to be addressed:

(1) The intrinsic correlation between the packing behavior of metallic atoms and mesoatoms remains a subject of investigation. Striking similarities in phase behavior have been observed between soft matter and transition metals, especially for elements like Cr, Mn, and Zn. However, certain significant phases (e.g., α-Mn, γ-brass) that should exist within the same theoretical frame are still missing in soft matter systems. The possibility of observing these phases in the future requires further exploration.

(2) The emergence of DQC demonstrates that a broad mesoatomic size distribution leads to unconventional phase behavior. Nevertheless, designing molecular systems with controlled mesoatomic polydispersity poses a significant challenge.

(3) All spherical packing phases introduced here are with metallic prototypes. This is partially because, metallic atoms that are generally regarded as spheres: protons and neutrons densely packed into atomic nuclei which is emerged in a cloud of free electrons. However, molecule-based mesoatoms may not be a perfect sphere due the restriction of molecular shape. When molecules stack together, the anisotropy was not only introduced in size distribution, but also shape distribution. As such, the packing rules of mesoatoms may deviate from that of metallic atoms. Such possibility paves the way to new structures beyond metal alloys.

To answer these questions, more GM systems are required to be designed and explored. The combination of multiple new characterization technologies (e.g., high-resolution transmission electron microscopy, single-molecule imaging, x-ray photon correlation spectroscopy, rheological characterization, as well as multiscale simulation) may be desirable to be incorporated in the future investigation of molecule-based spherical phases.

Concluding on a significant note, there has been considerable interest in the practical applications of soft materials featuring periodic structures. To create such materials, the dominant fabrication methods had been top-down technologies such as 3D printing [157,158] nanoimprint [159], and e-beam lithography [160]. Meanwhile, bottom-up strategies were primarily confined to the production of epitaxial lamellar or columnar structures [41]. However, the present GM-based alloylike structures now provide a controllable approach for generating soft superlattices on a larger scale. While the challenges in organic synthesis would still be a hurdle at the present stage, this advancement would serve as a potential material platform for manipulating photon/phonon properties, thus establishing an attractive foundation for the development of optical [1–3], acoustic/phononic [4,5], and mechanical [6,7] metamaterials.

[1] V. M. Shalaev, Nat. Photonics **1**, 41 (2007).
[2] H. Chen, C. T. Chan, and P. Sheng, Nat. Mater. **9**, 387 (2010).
[3] U. R. Gabinet and C. O. Osuji, Nano Res. **12**, 2172 (2019).
[4] R. Shnaiderman, G. Wissmeyer, O. Ulgen, Q. Mustafa, A. Chmyrov, and V. Ntziachristos, Nature (London) **585**, 372 (2020).
[5] Z. Wang, A. D. Christodoulides, L. Dai, Y. Zhou, R. Dai, Y. Xu, Q. Nian, J. Wang, J. A. Malen, and R. Y. Wang, Nano Lett. **22**, 4669 (2022).
[6] W. Shan, I. Weisbord, X. Feng, J. Hyon, G.-M. Manesi, A. Avgeropoulos, T. Segal-Peretz, and E. L. Thomas, Macromolecules **55**, 9022 (2022).
[7] S. Dhulipala, D. W. Yee, Z. Zhou, R. Sun, J. E. Andrade, R. J. Macfarlane, and C. M. Portela, Nano Lett. **23**, 5155 (2023).
[8] X. Yu, K. Yue, I. F. Hsieh, Y. Li, X. H. Dong, C. Liu, Y. Xin, H. F. Wang, A. C. Shi, G. R. Newkome *et al.*, Proc. Natl. Acad. Sci. USA **110**, 10078 (2013).
[9] Y. Rokhlenko, K. Kawamoto, J. A. Johnson, and C. O. Osuji, Macromolecules **51**, 3680 (2018).
[10] M. S. Ji, Q. Y. Guo, X. Y. Yan, Y. Liu, Y. J. Wu, K. Yue, and Z. H. Guo, Chemistry **27**, 7992 (2021).
[11] Z. H. Guo, A. N. Le, X. Feng, Y. Choo, B. Liu, D. Wang, Z. Wan, Y. Gu, J. Zhao, V. Li *et al.*, Angew. Chem. Int. Ed. **57**, 8493 (2018).
[12] G. von Freymann, V. Kitaev, B. V. Lotsch, and G. A. Ozin, Chem. Soc. Rev. **42**, 2528 (2013).
[13] J. Y. Cheng, C. A. Ross, H. I. Smith, and E. L. Thomas, Adv. Mater. **18**, 2505 (2006).
[14] W. Lu and C. M. Lieber, Nat. Mater. **6**, 841 (2007).
[15] Y. Liu, H. Lei, Q.-Y. Guo, X. Liu, X. Li, Y. Wu, W. Li, W. Zhang, G. Liu, X.-Y. Yan *et al.*, Chin. J. Polym. Sci. **41**, 607 (2023).
[16] S. Lee, C. Leighton, and F. S. Bates, Proc. Natl. Acad. Sci. USA **111**, 17723 (2014).
[17] V. S. K. Balagurusamy, G. Ungar, V. Percec, and G. Johansson, J. Am. Chem. Soc. **119**, 1539 (1997).
[18] S. A. Kim, K. J. Jeong, A. Yethiraj, and M. K. Mahanthappa, Proc. Natl. Acad. Sci. USA **114**, 4072 (2017).
[19] M. J. Huang, C. H. Hsu, J. Wang, S. Mei, X. H. Dong, Y. W. Li, M. X. Li, H. Liu, W. Zhang, T. Z. Aida *et al.*, Science **348**, 424 (2015).
[20] Z. B. Su, C. H. Hsu, Z. H. Gong, X. Y. Feng, J. B. Huang, R. M. Zhang, Y. Wang, J. L. Mao, C. Wesdemiotis, T. Li *et al.*, Nat. Chem. **11**, 899 (2019).
[21] R. J. Macfarlane, B. Lee, M. R. Jones, N. Harris, G. C. Schatz, and C. A. Mirkin, Science **334**, 204 (2011).
[22] X. Ye, C. Zhu, P. Ercius, S. N. Raja, B. He, M. R. Jones, M. R. Hauwiller, Y. Liu, T. Xu, and A. P. Alivisatos, Nat. Commun. **6**, 10052 (2015).
[23] M. A. Boles, M. Engel, and D. V. Talapin, Chem. Rev. **116**, 11220 (2016).
[24] I. Coropceanu, M. A. Boles, and D. V. Talapin, J. Am. Chem. Soc. **141**, 5728 (2019).
[25] Y. Tian, J. R. Lhermitte, L. Bai, T. Vo, H. L. Xin, H. Li, R. Li, M. Fukuto, K. G. Yager, J. S. Kahn *et al.*, Nat. Mater. **19**, 789 (2020).
[26] Q. Chen, S. C. Bae, and S. Granick, Nature (London) **469**, 381 (2011).
[27] M. He, J. P. Gales, E. Ducrot, Z. Gong, G. R. Yi, S. Sacanna, and D. J. Pine, Nature (London) **585**, 524 (2020).
[28] L. Zhang, J. B. Bailey, R. H. Subramanian, A. Groisman, and F. A. Tezcan, Nature (London) **557**, 86 (2018).
[29] Z. Lin, H. Emamy, B. Minevich, Y. Xiong, S. Xiang, S. Kumar, Y. Ke, and O. Gang, J. Am. Chem. Soc. **142**, 17531 (2020).
[30] B. E. Partridge, P. H. Winegar, Z. Han, and C. A. Mirkin, J. Am. Chem. Soc. **143**, 8925 (2021).

[31] K. Kim, M. W. Schulze, A. Arora, R. M. Lewis III, M. A. Hillmyer, K. D. Dorfman, and F. S. Bates, Science **356**, 520 (2017).

[32] A. Jayaraman, D. Y. Zhang, B. L. Dewing, and M. K. Mahanthappa, Acs Cent. Sci. **5**, 619 (2019).

[33] X. Y. Yan, Q. Y. Guo, Z. Lin, X. Y. Liu, J. Yuan, J. Wang, H. Wang, Y. Liu, Z. Su, T. Liu *et al.*, Angew. Chem. Int. Ed. **60**, 2024 (2021).

[34] Q. Y. Guo, X. Y. Yan, W. Zhang, X. H. Li, Y. Xu, S. Dai, Y. Liu, B. X. Zhang, X. Feng, J. Yin *et al.*, J. Am. Chem. Soc. **143**, 12935 (2021).

[35] J. Ren, T. Segal-Peretz, C. Zhou, G. S. W. Craig, and P. F. Nealey, Sci. Adv. **6**, eaaz0002 (2020).

[36] A. Reddy, M. B. Buckley, A. Arora, F. S. Bates, K. D. Dorfman, and G. M. Grason, Proc. Natl. Acad. Sci. **115**, 10233 (2018).

[37] H. Shin, M. J. Bowick, and X. Xing, Phys. Rev. Lett. **101**, 037802 (2008).

[38] G. M. Grason and E. L. Thomas, Phys. Rev. Mater. **7**, 045603 (2023).

[39] F. S. Bates and G. H. Fredrickson, Phys. Today **52**(2), 32 (1999).

[40] F. S. Bates, M. A. Hillmyer, T. P. Lodge, C. M. Bates, K. T. Delaney, and G. H. Fredrickson, Science **336**, 434 (2012).

[41] S. B. Darling, Prog. Polym. Sci. **32**, 1152 (2007).

[42] Y. Y. Mai and A. Eisenberg, Chem. Soc. Rev. **41**, 5969 (2012).

[43] A. J. Meuler, M. A. Hillmyer, and F. S. Bates, Macromolecules **42**, 7221 (2009).

[44] C. Park, J. Yoon, and E. L. Thomas, Polymer **44**, 6725 (2003).

[45] W.-B. Zhang, X. Yu, C.-L. Wang, H.-J. Sun, I. F. Hsieh, Y. Li, X.-H. Dong, K. Yue, R. Van Horn, and S. Z. D. Cheng, Macromolecules **47**, 1221 (2014).

[46] W. Zhang, Y. Liu, J. Huang, T. Liu, W. Xu, S. Z. D. Cheng, and X. H. Dong, Soft Matter **15**, 7108 (2019).

[47] W. B. Zhang and S. Z. D. Cheng, Giant **1**, 100011 (2020).

[48] Z. B. Su, R. M. Zhang, X. Y. Yan, Q. Y. Guo, J. H. Huang, W. P. Shan, Y. C. Liu, T. Liu, M. J. Huang, and S. Z. D. Cheng, Prog. Polym. Sci. **103**, 101230 (2020).

[49] R. Zhang, Z. Su, X. Y. Yan, J. Huang, W. Shan, X. H. Dong, X. Feng, Z. Lin, and S. Z. D. Cheng, Chemistry **26**, 6741 (2020).

[50] X. Y. Yan, Q. Y. Guo, X. Y. Liu, Y. C. Wang, J. Wang, Z. B. Su, J. H. Huang, F. G. Bian, H. X. Lin, M. J. Huang *et al.*, J. Am. Chem. Soc. **143**, 21613 (2021).

[51] T. Wen, B. Ni, Y. Liu, W. Zhang, Z.-H. Guo, Y.-C. Lee, R.-M. Ho, and S. Z. D. Cheng, Giant **8**, 100078 (2021).

[52] H. Lei, Y. Liu, T. Liu, Q. Y. Guo, X. Y. Yan, Y. Wang, W. Zhang, Z. Su, J. Huang, W. Xu *et al.*, Angew. Chem. Int. Ed. **61**, e202203433 (2022).

[53] Y. C. Liu, T. Liu, X. Y. Yan, Q. Y. Guo, H. Y. Lei, Z. W. Huang, R. Zhang, Y. Wang, J. Wang, F. Liu *et al.*, Proc. Natl. Acad. Sci. USA **119**, e2115304119 (2022).

[54] Y. C. Wang, J. H. Huang, X. Y. Yan, H. Y. Lei, X. Y. Liu, Q. Y. Guo, Y. C. Liu, T. Liu, M. J. Huang, F. G. Bian *et al.*, Angew. Chem. Int. Ed. **61**, e202200637 (2022).

[55] W. Xu, Y. Wang, Q.-Y. Guo, X. Wang, Y. Liu, F.-G. Bian, X.-Y. Yan, B. Ni, and S. Z. D. Cheng, Polym. Chem. **13**, 2108 (2022).

[56] H. Lei, X.-H. Li, Y. Liu, X.-Y. Liu, W.-Y. Li, X.-Y. Yan, M. Huang, S. Z. D. Cheng, and J. Huang, Thermochim. Acta **719**, 179411 (2023).

[57] X.-H. Dong, B. Ni, M. Huang, C.-H. Hsu, Z. Chen, Z. Lin, W.-B. Zhang, A.-C. Shi, and S. Z. D. Cheng, Macromolecules **48**, 7172 (2015).

[58] Z. Lin, P. Lu, C.-H. Hsu, J. Sun, Y. Zhou, M. Huang, K. Yue, B. Ni, X.-H. Dong, X. Li *et al.*, Macromolecules **48**, 5496 (2015).

[59] K. Yue, M. J. Huang, R. L. Marson, J. L. He, J. H. Huang, Z. Zhou, J. Wang, C. Liu, X. S. Yan, K. Wu *et al.*, Proc. Natl. Acad. Sci. USA **113**, 14195 (2016).

[60] W. Zhang, M. J. Huang, H. Su, S. Y. Zhang, K. Yue, X. H. Dong, X. P. Li, H. Liu, S. Zhang, C. Wesdemiotis *et al.*, ACS Cent. Sci. **2**, 48 (2016).

[61] X. Y. Feng, R. M. Zhang, Y. W. Li, Y. L. Hong, D. Guo, K. Lang, K. Y. Wu, M. J. Huang, J. L. Mao, C. Wesdemiotis *et al.*, Acs Cent. Sci. **3**, 860 (2017).

[62] Z. W. Lin, X. Yang, H. Xu, T. Sakurai, W. Matsuda, S. Seki, Y. B. Zhou, J. Sun, K. Y. Wu, X. Y. Yan *et al.*, J. Am. Chem. Soc. **139**, 18616 (2017).

[63] W. Zhang, X. L. Lu, J. L. Mao, C. H. Hsu, G. Y. Mu, M. J. Huang, Q. Y. Guo, H. Liu, C. Wesdemiotis, T. Li *et al.*, Angew. Chem. Int. Ed. **56**, 15014 (2017).

[64] X. Feng, G. Liu, D. Guo, K. Lang, R. Zhang, J. Huang, Z. Su, Y. Li, M. Huang, T. Li *et al.*, ACS Macro. Lett. **8**, 875 (2019).

[65] B. Ni, H. R. Qu, J. L. Mao, R. B. Bai, S. L. Zhang, X. Y. Feng, C. Wesdemiotis, X. H. Dong, and S. Z. D. Cheng, Polymer **167**, 118 (2019).

[66] R. M. Zhang, X. Y. Feng, R. Zhang, W. P. Shan, Z. B. Su, J. L. Mao, C. Wesdemiotis, J. H. Huang, X. Y. Yan, T. Liu *et al.*, Angew. Chem. Int. Ed. **58**, 11879 (2019).

[67] J. H. Huang, Z. B. Su, M. J. Huang, R. C. Zhang, J. Wang, X. Y. Feng, R. Zhang, R. M. Zhang, W. P. Shan, X. Y. Yan *et al.*, Angew. Chem. Int. Ed. **59**, 18563 (2020).

[68] J. Jiang, Y. Wang, L. Jin, C. H. Hsu, S. L. Zhang, J. L. Mao, W. B. Yin, T. Li, B. Ni, Z. B. Su *et al.*, ACS Appl. Nano Mater. **3**, 2952 (2020).

[69] Y. C. Liu, T. Liu, X. Y. Yan, Q. Y. Guo, J. Wang, R. C. Zhang, S. L. Zhang, Z. B. Su, J. H. Huang, G. X. Liu *et al.*, Giant **4**, 100031 (2020).

[70] J. H. Huang, R. M. Zhang, Y. C. Wang, Z. B. Su, X. Y. Yan, Q. Y. Guo, T. Liu, Y. C. Liu, H. Y. Lei, M. J. Huang *et al.*, Macromolecules **54**, 7777 (2021).

[71] Z. B. Su, J. H. Huang, W. P. Shan, X. Y. Yan, R. M. Zhang, T. Liu, Y. C. Liu, Q. Y. Guo, F. G. Bian, X. R. Miao *et al.*, Ccs Chem. **3**, 1434 (2021).

[72] X. Y. Yan, Z. Lin, W. Zhang, H. Xu, Q. Y. Guo, Y. Liu, J. Luo, X. Y. Liu, R. Zhang, J. Huang *et al.*, Angew. Chem. Int. Ed. **59**, 5226 (2020).

[73] G. K. Cheong, F. S. Bates, and K. D. Dorfman, Proc. Natl. Acad. Sci. USA **117**, 16764 (2020).

[74] N. Xie, W. Li, F. Qiu, and A. C. Shi ACS Macro. Lett. **3**, 906 (2014).

[75] W. Li, C. Duan, and A. C. Shi, ACS Macro. Lett. **6**, 1257 (2017).

[76] R. A. LaCour, C. S. Adorf, J. Dshemuchadse, and S. C. Glotzer, ACS Nano **13**, 13829 (2019).

[77] A. Travesset, Phys. Rev. Lett. **119**, 115701 (2017).

[78] Y.-Y. Huang, H.-L. Chen, and T. Hashimoto, Macromolecules **36**, 764 (2003).

[79] Y.-Y. Huang, J.-Y. Hsu, H.-L. Chen, and T. Hashimoto, Macromolecules **40**, 3700 (2007).

[80] K. Mortensen, W. Batsberg, and S. Hvidt, Macromolecules **41**, 1720 (2008).

[81] O. Kim, S. Y. Kim, J. Lee, and M. J. Park, Chem. Mater. **28**, 318 (2015).

[82] L. Chen, H. S. Lee, and S. Lee, Proc. Natl. Acad. Sci. USA **115**, 7218 (2018).

[83] L.-T. Chen, C.-Y. Chen, and H.-L. Chen, Polymer **169**, 131 (2019).

[84] L.-T. Chen, Y.-T. Huang, C.-Y. Chen, M.-Z. Chen, and H.-L. Chen, Macromolecules **54**, 8936 (2021).

[85] N.-W. Hsu, B. Nouri, L.-T. Chen, and H.-L. Chen, Macromolecules **53**, 9665 (2020).

[86] C. Zhang, D. L. Vigil, D. Sun, M. W. Bates, T. Loman, E. A. Murphy, S. M. Barbon, J. A. Song, B. Yu, G. H. Fredrickson *et al.*, J. Am. Chem. Soc. **143**, 14106 (2021).

[87] A. Jayaraman and M. K. Mahanthappa, Langmuir **34**, 2290 (2018).

[88] A. J. Mueller, A. P. Lindsay, A. Jayaraman, S. Weigand, T. P. Lodge, M. K. Mahanthappa, and F. S. Bates, Macromolecules **55**, 8332 (2022).

[89] S. Jeon, T. Jun, S. Jo, K. Kim, B. Lee, S. Lee, and D. Y. Ryu, Macromolecules **55**, 8049 (2022).

[90] S. Lee, M. J. Bluemle, and F. S. Bates, Science **330**, 349 (2010).

[91] V. Percec, W.-D. Cho, G. Ungar, and D. J. P. Yeardley, J. Am. Chem. Soc. **123**, 1302 (2001).

[92] V. Percec, C. H. Ahn, G. Ungar, D. J. P. Yeardley, M. Möller, and S. S. Sheiko, Nature (London) **391**, 161 (1998).

[93] S. D. Hudson, H. T. Jung, V. Percec, W. D. Cho, G. Johansson, G. Ungar, and V. S. K. Balagurusamy, Science **278**, 449 (1997).

[94] D. V. Perroni and M. K. Mahanthappa, Soft Matter **9**, 7919 (2013).

[95] V. Percec, W. D. Cho, P. E. Mosier, G. Ungar, and D. J. P. Yeardley, J. Am. Chem. Soc. **120**, 11061 (1998).

[96] V. Percec, W.-D. Cho, M. Möller, S. A. Prokhorova, G. Ungar, and D. J. P. Yeardley, J. Am. Chem. Soc. **122**, 4249 (2000).

[97] V. Percec, W.-D. Cho, G. Ungar, and D. J. P. Yeardley, Angew. Chem. Int. Ed. **39**, 1597 (2000).

[98] V. Percec, C. M. Mitchell, W. D. Cho, S. Uchida, M. Glodde, G. Ungar, X. Zeng, Y. Liu, V. S. Balagurusamy, and P. A. Heiney, J. Am. Chem. Soc. **126**, 6078 (2004).

[99] V. Percec, M. Peterca, M. J. Sienkowska, M. A. Ilies, E. Aqad, J. Smidrkal, and P. A. Heiney, J. Am. Chem. Soc. **128**, 3324 (2006).

[100] V. Percec, M. R. Imam, M. Peterca, D. A. Wilson, R. Graf, H. W. Spiess, V. S. Balagurusamy, and P. A. Heiney, J. Am. Chem. Soc. **131**, 7662 (2009).

[101] V. Percec, M. R. Imam, M. Peterca, D. A. Wilson, and P. A. Heiney, J. Am. Chem. Soc. **131**, 1294 (2009).

[102] B. M. Rosen, D. A. Wilson, C. J. Wilson, M. Peterca, B. C. Won, C. Huang, L. R. Lipski, X. Zeng, G. Ungar, P. A. Heiney *et al.*, J. Am. Chem. Soc. **131**, 17500 (2009).

[103] B. M. Rosen, M. Peterca, C. Huang, X. Zeng, G. Ungar, and V. Percec, Angew. Chem. Int. Ed. **49**, 7002 (2010).

[104] M. Peterca, M. R. Imam, S. D. Hudson, B. E. Partridge, D. Sahoo, P. A. Heiney, M. L. Klein, and V. Percec, ACS Nano **10**, 10480 (2016).

[105] M. N. Holerca, D. Sahoo, B. E. Partridge, M. Peterca, X. Zeng, G. Ungar, and V. Percec, J. Am. Chem. Soc. **140**, 16941 (2018).

[106] D. A. Wilson, K. A. Andreopoulou, M. Peterca, P. Leowanawat, D. Sahoo, B. E. Partridge, Q. Xiao, N. Huang, P. A. Heiney, and V. Percec, J. Am. Chem. Soc. **141**, 6162 (2019).

[107] N. Huang, M. R. Imam, M. J. Sienkowska, M. Peterca, M. N. Holerca, D. A. Wilson, B. M. Rosen, B. E. Partridge, Q. Xiao, and V. Percec, Giant **1**, 100001 (2020).

[108] S. Chanpuriya, K. Kim, J. Zhang, S. Lee, A. Arora, K. D. Dorfman, K. T. Delaney, G. H. Fredrickson, and F. S. Bates, ACS Nano **10**, 4961 (2016).

[109] A. B. Chang and F. S. Bates, ACS Nano **14**, 11463 (2020).

[110] K. K. Lachmayr and L. R. Sita, Angew. Chem. Int. Ed. **59**, 3563 (2020).

[111] K. K. Lachmayr, C. M. Wentz, and L. R. Sita, Angew. Chem. Int. Ed. **59**, 1521 (2020).

[112] A. P. Lindsay, R. M. Lewis 3rd, B. Lee, A. J. Peterson, T. P. Lodge, and F. S. Bates, ACS Macro. Lett. **9**, 197 (2020).

[113] M. W. Bates, J. Lequieu, S. M. Barbon, R. M. Lewis 3rd, K. T. Delaney, A. Anastasaki, C. J. Hawker, G. H. Fredrickson, and C. M. Bates, Proc. Natl. Acad. Sci. USA **116**, 13194 (2019).

[114] G. Ungar, Y. Liu, X. Zeng, V. Percec, and W. D. Cho, Science **299**, 1208 (2003).

[115] M. N. Holerca, D. Sahoo, M. Peterca, B. E. Partridge, P. A. Heiney, and V. Percec, Macromolecules **50**, 375 (2016).

[116] V. Percec, N. Huang, Q. Xiao, B. E. Partridge, D. Sahoo, M. R. Imam, M. Peterca, R. Graf, H.-W. Spiess, X. Zeng *et al.*, Giant **9**, 100084 (2022).

[117] M. W. Schulze, R. M. Lewis, J. H. Lettow, R. J. Hickey, T. M. Gillard, M. A. Hillmyer, and F. S. Bates, Phys. Rev. Lett. **118**, 207801 (2017).

[118] A. P. Lindsay, G. K. Cheong, A. J. Peterson, S. Weigand, K. D. Dorfman, T. P. Lodge, and F. S. Bates, Macromolecules **54**, 7088 (2021).

[119] C. M. Baez-Cotto and M. K. Mahanthappa, ACS Nano **12**, 3226 (2018).

[120] K. Kim, A. Arora, R. M. Lewis, III, M. Liu, W. Li, A. C. Shi, K. D. Dorfman, and F. S. Bates, Proc. Natl. Acad. Sci. USA **115**, 847 (2018).

[121] T. Jun, H. Park, S. Jeon, S. Jo, H. Ahn, W. D. Jang, B. Lee, and D. Y. Ryu, J. Am. Chem. Soc. **143**, 17548 (2021).

[122] X.-H. Li, X. Kuang, X.-Y. Liu, H. Lei, X.-Y. Yan, W. Li, Y. Deng, Y. Wu, Q.-Y. Guo, and S. Z. D. Cheng, Giant **16**, 100196 (2023).

[123] A. J. Mueller, A. P. Lindsay, A. Jayaraman, T. P. Lodge, M. K. Mahanthappa, and F. S. Bates, ACS Macro. Lett. **9**, 576 (2020).

[124] S. Xie, B. Zhang, F. S. Bates, and T. P. Lodge, Macromolecules **54**, 6990 (2021).

[125] X. Zeng, G. Ungar, Y. Liu, V. Percec, A. E. Dulcey, and J. K. Hobbs, Nature (London) **428**, 157 (2004).

[126] T. M. Gillard, S. Lee, and F. S. Bates, Proc. Natl. Acad. Sci. USA **113**, 5167 (2016).

[127] J. Zhang and F. S. Bates, J. Am. Chem. Soc. **134**, 7636 (2012).

[128] A. Jayaraman, C. M. Baez-Cotto, T. J. Mann, and M. K. Mahanthappa, Proc. Natl. Acad. Sci. USA **118**, e2101598118 (2021).

[129] M. R. Imam, M. Peterca, Q. Xiao, and V. Percec, Giant **10**, 100098 (2022).

[130] D. Sahoo, M. Peterca, M. R. Imam, B. E. Partridge, Q. Xiao, and V. Percec, Giant **10**, 100096 (2022).
[131] A. P. Lindsay, A. Jayaraman, A. J. Peterson, A. J. Mueller, S. Weigand, K. Almdal, M. K. Mahanthappa, T. P. Lodge, and F. S. Bates, ACS Nano **15**, 9453 (2021).
[132] A. J. Mueller, A. P. Lindsay, A. Jayaraman, T. P. Lodge, M. K. Mahanthappa, and F. S. Bates, Macromolecules **54**, 2647 (2021).
[133] X. Ye, J. Chen, M. Eric Irrgang, M. Engel, A. Dong, S. C. Glotzer, and C. B. Murray, Nat. Mater. **16**, 214 (2017).
[134] S. Abbas and T. P. Lodge, Phys. Rev. Lett. **97**, 097803 (2006).
[135] M. D. Graef and M. E. Mchenry, *Structure of Materials: An Introduction to Crystallography, Diffraction, and Symmetry*, 2nd ed. (Cambridge University Press, Cambridge, 2012).
[136] J. H. Conway and N. J. A. Sloane, *Sphere Packings, Lattices, and Groups*, 3rd ed. (Springer-Verlag., New York, 1999).
[137] T. C. Hales, in *The Kepler Conjecture*, edited by J. C. Lagarias (Springer, New York, 2011), pp. 65.
[138] M. Watzlawek, C. N. Likos, and H. Löwen, Phys. Rev. Lett. **82**, 5289 (1999).
[139] B. Groh and M. Schmidt, J. Chem. Phys. **114**, 5450 (2001).
[140] D. Weaire and R. Phelan, Philos. Mag. Lett. **69**, 107 (1994).
[141] F. C. Frank and J. S. Kasper, Acta Crystallogr. **11**, 184 (1958).
[142] F. C. Frank and J. S. Kasper, Acta Crystallogr. **12**, 483 (1959).
[143] H. Xie, J. Bai, H. Ren, S. Li, H. Pan, Y. Ren, and G. Qin, Nano Lett. **21**, 7198 (2021).
[144] M. Dutour Sikiric, O. Delgado-Friedrichs, and M. Deza, Acta Crystallogr. A **66**, 602 (2010).
[145] V. Tournier, C. M. Topham, A. Gilles, B. David, C. Folgoas, E. Moya-Leclair, E. Kamionka, M. L. Desrousseaux, H. Texier, S. Gavalda *et al.*, Nature (London) **580**, 216 (2020).
[146] E. Ducrot, M. He, G. R. Yi, and D. J. Pine, Nat. Mater. **16**, 652 (2017).
[147] R. Gabbrielli, A. J. Meagher, D. Weaire, K. A. Brakke, and S. Hutzler, Philos. Mag. Lett. **92**, 1 (2012).
[148] D. Levine and P. J. Steinhardt, Phys. Rev. Lett. **53**, 2477 (1984).
[149] W. Steurer and J. Dshemuchadse, *Intermetallics Structures, Properties, and Statistics* (Oxford University Press, Oxford, 2016).
[150] A. L. Mackay, Acta Crystallogr. **15**, 916 (1962).
[151] A. P. Tsai, J. Q. Guo, E. Abe, H. Takakura, and T. J. Sato, Nature (London) **408**, 537 (2000).
[152] G. Ungar and X. Zeng, Soft Matter **1**, 95 (2005).
[153] D. R. Nelson, Phys. Rev. B **28**, 5515 (1983).
[154] V. Percec, W.-D. Cho, and G. Ungar, J. Am. Chem. Soc. **122**, 10273 (2000).
[155] B. M. Rosen, C. J. Wilson, D. A. Wilson, M. Peterca, M. R. Imam, and V. Percec, Chem. Rev. **109**, 6275 (2009).
[156] A. Reddy and G. M. Grason, Nat. Chem. **11**, 865 (2019).
[157] M. Regehly, Y. Garmshausen, M. Reuter, N. F. Konig, E. Israel, D. P. Kelly, C. Y. Chou, K. Koch, B. Asfari, and S. Hecht, Nature (London) **588**, 620 (2020).
[158] J. Bauer, C. Crook, and T. Baldacchini, Science **380**, 960 (2023).
[159] L. J. Guo, Adv. Mater. **19**, 495 (2007).
[160] A. E. Grigorescu and C. W. Hagen, Nanotechnology **20**, 292001 (2009).